Received: 15 April 2021 | Accepted: 6 June 2021

DOI: 10.1002/mma.7651

RESEARCH ARTICLE

WILEY

Quantitative analysis of total magnetic anomaly maps on archaeological sites—Part 2

Hazel Deniz Toktay | **Davut Aydoğan** | **Fethi Ahmet Yüksel**

Geophysical Engineering Department, Istanbul University- Cerrahpasa, Istanbul, Turkey

Correspondence
Hazel Deniz Toktay, Geophysical Engineering Department, Istanbul University- Cerrahpasa, Istanbul, Turkey.
Email: hazel.deniztoktay@iuc.edu.tr

Communicated by: M. Efendiev

In this study, which is the second part of quantitative analysis of total magnetic anomaly maps on archaeological sites, it is aimed to analyze the depth values of potential buried structures that cause anomalies from the total magnetic anomaly maps of an archaeological excavation area. In the first step, depth values of the structures whose boundaries were determined on the improved total magnetic anomaly map of the model were analyzed. Depth values of blocks were calculated by using of tilt angle depth (TAD), source parameter imaging (SPI), and improved source parameter imaging (iSPI) methods. In the second step, the depth values at these boundaries were calculated. The total magnetic anomaly map of the mound area, for which the structure boundary analysis was made was calculated, and the depth values at the potential structure boundaries were calculated. Finally, the depth values are visualized on the simplified structure map of the region by combining and simplifying the potential structure boundary locations.

KEYWORDS

geophysics, quantitative analysis, source parameter imaging, tilt angle depth, total magnetic anomaly map

MSC CLASSIFICATION

86A04; 86A20

1 | INTRODUCTION

Analysis of the depth values of effective sources that cause geophysical anomalies has an important place in engineering and exploration studies to take maximum information. The heterogeneous structure of the subsurface makes it challenging to identify and interpret the buried structures. Depths, locations, continuations, and distributions of potential subsurface structures can be accurately determined using derivative-based methods to anomaly maps obtained by the magnetic method. Various methods have been used for interpreting magnetic data such as, Euler deconvolution,[1] the least squares method,[2] wavelet method,[3] depth from extreme points (DEXP) method,[4] SLUTH method,[5] and maximum structural index method.[6] In this paper, the depth values have been determined by using tilt angle depth (TAD), source parameter imaging (SPI), and improved SPI (iSPI) methods. In the first stage, to test the accuracy of these methods with

Abbreviations: iSPI, improved source parameter imaging; SPI, source parameter imaging; TAD, tilt angle depth.

actual field data, a synthetic model was created compatible with the archaeological structures. The depth values of the synthetic model blocks were analyzed by applying TAD, SPI, and iSPI methods to the total magnetic anomaly map of the model. In the second stage, similar quantitative analyses have been made on the total magnetic anomaly map of actual field data, and the depth values of potential structures are determined.

2 | DEPTH CALCULATIONS

2.1 | Tilt angle depth method

The TAD method is one of the most widely used methods applied in archaeogeophysical study areas to determine the vertical discontinuities of potential subsurface structures. This method was created by developing the derivative-based tilt angle method, which is used to find the horizontal boundaries of the structures for vertical discontinuities. The tilt angle method was first described by Miller and Singh,[7] and later Verduzco et al.[8] and Salem et al.,[9] indicating the derivatives of the total magnetic field (M) data in the x, y, and z directions as (Equation 1),

$$\frac{\partial M}{\partial x}, \frac{\partial M}{\partial y}, \text{ and } \frac{\partial M}{\partial z} \tag{1}$$

and rearranged by placing the expressions in total horizontal derivative and vertical derivative expressions.[7] The total horizontal derivative is calculated as the square root of the sum of the squares of the derivatives of the magnetic field in the x and y direction, from the Equation (2) as

$$\frac{\partial M}{\partial h} = \sqrt{\left(\frac{\partial M}{\partial x}^2\right) + \left(\frac{\partial M}{\partial y}^2\right)} \tag{2}$$

where $(\partial M/\partial x)$ denotes the magnetic field derivative in the x direction and $(\partial M/\partial y)$ denotes the magnetic field derivative in the y direction.

Many features of the tilt angle method are used in the application stage. For example, due to the nature of the arctangent function, all tilt amplitudes are limited to (−90°, 90°) regardless of the value of the total horizontal derivative or the amplitude value of the vertical gradient. It can be seen that the tilt angle is superior to automatic gain control, although it is calculated similarly. The tilt angle method equalizes the amplitudes of magnetic anomalies along the grid or profile. It preserves the spectral integrity of the signal by enabling advanced numerical analysis (for example, determining the local wave number).

Equations for the vertical and horizontal derivatives of the magnetic field on the fault at the horizontal location $h = 0$ and depth z_c of the method in question are given by Nabighian[10] as,

$$\frac{\partial M}{\partial h} = 2KF_c\, sind\, \frac{z_c cos\,(2I - d - 90) + hsin\,(2I - d - 90)}{h^2 + z_c{}^2} \tag{3}$$

$$\frac{\partial M}{\partial z} = 2KF_c\, sind \frac{hcos\,(2I - d - 90) - z_c sin\,(2I - d - 90)}{h^2 + z_c{}^2} \tag{4}$$

where K is the susceptibility difference in the fault, F is the magnetic field magnitude, $c = 1 - cos2isin2A$, A is the angle between the magnetic north and the positive vertical axis (h), i is the inclination angle of the surrounding area, $tanI = tani/cosA$, d is the dip (measured from vertical axis) measured from the axis. axis. In approximations where the magnetic field or fault structure is nearly vertical, Equations of 3 and 4 transform to Equations 5 and 6 below.

$$\frac{\partial M}{\partial h} = 2KF_c\, sind\, \frac{z_c}{h^2 + z_c{}^2} \tag{5}$$

$$\frac{\partial M}{\partial z} = 2KFc\, sind\, \frac{h}{h^2 + z_c{}^2} \tag{6}$$

TAD Equation (7) is determined by substituting the Equations (5) and (6) in the tilt angle equation.

$$\theta = tan^{-1}\left(\frac{h}{z_c}\right) \tag{7}$$

The value of the inclination angle is 0° when the boundaries of the source are ($h = 0$), 45° when $h = +z_c$, and −45° when $h = -z_c$. In other words, if $h = \pm z_c$ and $\theta = \pm 45$ in the last two equations, the location and depth of the anomaly along the tilt angle maps can be calculated by carefully measuring the contour intervals.

2.2 | Source parameter imaging method

SPI method is a method first defined by Thurston and Smith.[11] The depth of the magnetic source and the differences in dip and susceptibility can be calculated using this method. The dipolar behavior of the magnetic potential makes it challenging to define characteristic points.[11] In order to reduce this effect, source parameters deconvolved from magnetic potential are used in the SPI method. Methods such as Naudy method, Werner's method, and Euler method are applied to the data obtained on the determined magnetic profiles. However, these methods are used in 2-D structures and require correction for the distinct layer direction depending on the profile direction. Grid-based methods such as 3-D Euler and 3-D analytical signals have been developed. These methods have a more advantageous structure than profile methods since they do not require a correction related to the direction of the source. The advantage of grid-based methods is that profiles perpendicular to 2-D structures are not required.

Although the SPI method is applied to digitized data, it still has some restrictions. This method assumes that the observed area is caused by the susceptibility difference caused by the 2-D dipping fault or the 2-D thin dike structure and that there is no residual magnetization in the dip and susceptibility estimates. However, the depth estimation is independent of magnetic inclination, declination, and residual magnetization. Another advantage of the method is that it produces results without defining the window size as in Naudy and Euler methods. Later, the output images obtained can be used to improve the structural details. Thurston and Smith[11s]howed in their study that the SPI method is an extended version of the complex analytical signal theory since it calculates three properties in addition to the local amplitude, local phase, and local frequency where the source parameters can be calculated.

In this model-dependent method, the selected model can only be changed with the values entered as input data to the algorithm. Then, the advantage of the method is that the depth parameter can be calculated using the complex analytical signal without the need for magnetization direction information. The complex analytic signal can be shown as,[10]

$$A(x,z) = \frac{\partial M(x,z)}{\partial x} - j\frac{\partial M(x,z)}{\partial z} \tag{8}$$

where $M(x,z)$ is the total magnetic field magnitude and j is an imaginary number. Analytical signal amplitude ($|A|$) and local phase (θ) equations are given below.

$$|A| = \sqrt{\left(\frac{\partial M}{\partial x}\right)^2 + \left(\frac{\partial M}{\partial z}\right)^2} \tag{9}$$

$$\theta = tan^{-1}\left(\frac{\frac{\partial M}{\partial z}}{\frac{\partial M}{\partial x}}\right) \tag{10}$$

Putting these expressions in Equation (7), the equation of

$$A(x,z) = |A|\exp(j\theta) \tag{11}$$

is reached. In the SPI method, the local frequency is the parameter that shows the change of the local phase with respect to x. If it is shown with f, the equation that contains the vertical and horizontal derivatives of the field is obtained[12] (Equation 12).

$$f = \frac{1}{2\pi}\frac{\partial}{\partial x}\, tan^{-1}\left[\frac{\frac{\partial M}{\partial z}}{\frac{\partial M}{\partial x}}\right] \tag{12}$$

The relationship between local wave number (κ) and local frequency (f) has been described as follows.

$$\kappa = 2\pi f \tag{13}$$

The equation obtained by substituting Equation (13) in Equation (12) is shown as follows:

$$\kappa = \frac{1}{|A|^2}\left(\frac{\partial^2 M}{\partial x \partial z}\frac{\partial M}{\partial x} - \frac{\partial^2 M}{\partial x^2}\frac{\partial M}{\partial z}\right) \tag{14}$$

When analytical expressions of the vertical and horizontal derivatives of a sloping fault are put in place in Equation (14), the local wave number expression can be rewritten as follows in order to examine how complex features are used to directly calculate edge locations, depth, dip, and susceptibility difference.

$$\kappa = \frac{h}{h^2 + x^2} \tag{15}$$

In Equation (15), h represents the depth of the upper surface of the fault. In the coordinate system, the x value region equal to 0 is located directly on the boundary of the source. This equation is proof that the maximum points of the local number of waves are independent of the magnetization direction. Thus, the peaks in the anomaly reveal the source edges, and in these regions, $x = 0$, the local depth at this point can be calculated by the equation of the following.

$$h = \frac{1}{\kappa} \tag{16}$$

While local depth, dip, and susceptibility are obtained, it is accepted that surrounding anomalies do not cause any effect. Such effects distort the results obtained from all applied automatic algorithms and generally require more detailed modeling in order to make a more accurate numerical analysis. However, using a second-order derivative to obtain images in this method is much less interactive than using the total field or first derivative.

2.3 | Improved source parameter imaging method

The interpretation of magnetic anomalies involves calculating physical and geometric parameters that characterize the source causing the anomaly. The top depth value of the source can be calculated by applying the SPI method. One advantage of the SPI method is that depths are visually imagined. Generally, this image is for a fault pattern or a dike pattern. The depth estimation obtained depends on the default model.

The iSPI was created by expanding the SPI method by adding a horizontal cylinder model. At the same time, the method allows automatically determining the most suitable model. The selected model can be visualized, and accurate depth estimation can be made for each anomaly. Therefore, effective source depths can be shown by mapping independently of the assumed model. iSPI method allows more accessible analysis of theoretical and field data.

The method analyzes the analytical signal response and the properties of the second derivative responses of the analytical signal. The most suitable model can be determined from this analysis, and depth estimation can be made independent of the assumptions about the model. As with the SPI method, this method can also be applied to fault and dike type geological models. In the iSPI method, the interpretation process has been made easier by adding the horizontal cylinder model and the fault and dike structures.

iSPI method is an analytical signal concept that includes second derivatives of the total magnetic field.[13] The second-order derivative expression of the analytical signal ($A_2(x, z)$) can be expressed by the equation as follows.

$$A_2(x, z) = \frac{\partial^2 M(x, z)}{\partial x \partial z} - j\frac{\partial^2 M(x, z)}{\partial^2 z} \tag{17}$$

By using expression (17), the second-order local wave number (κ_2) is given as follows.

$$\kappa_2 = \frac{\partial}{\partial x} tan^{-1} \left[\frac{\frac{\partial^2 M}{\partial^2 z}}{\frac{\partial^2 M}{\partial z \partial x}} \right] \tag{18}$$

First- and second-order local wave numbers can determine the most suitable model and determine the depth without being dependent on any assumptions about the model. If vertical and horizontal gradient equations of the long horizontal cylinder,[14] dike,[15] and fault models[10] are put into place in the first- and second-order local wave number equations, the new local wave number equations can be obtained as,

$$\kappa_1 = \frac{(n_k + 1)\, h_k}{{h_k}^2 + x^2} \tag{19}$$

$$\kappa_2 = \frac{(n_k + 2)\, h_k}{{h_k}^2 + x^2} \tag{20}$$

where n_k is the SPI structure index (subscript $k = c$, t, or h). SPI structure indexes have $n_c = 0$ for the fault model, $n_t = 1$ for the thin dike model, and $n_h = 2$ for the horizontal cylinder model. As shown in the obtained relations, first- and second-order local wave number expressions are independent of susceptibility difference, dip angle, inclination, equation angles, and ground magnetic field. Local wave numbers (κ_1 and κ_2) are in the same functional form for the three models. In any case, at the point $x = 0$, the function values are symmetric and take the maximum value at the source boundaries. Here, the point $x = 0$ defines the location of the source and can be easily obtained from the local wave numbers. The only difference between the local wave numbers κ_1 and κ_2 is the change in the amplitude factor related to the structural index n_k.

The model-independent local wave number value can be calculated by the difference of the first-order local wave numbers and the second-order local wave numbers ($\kappa_2 - \kappa_1$). The area where this function reaches its maximum (at $x = 0$) always gives the value of $1/h_k$, and it is in the same functional form in all three models. The only difference between

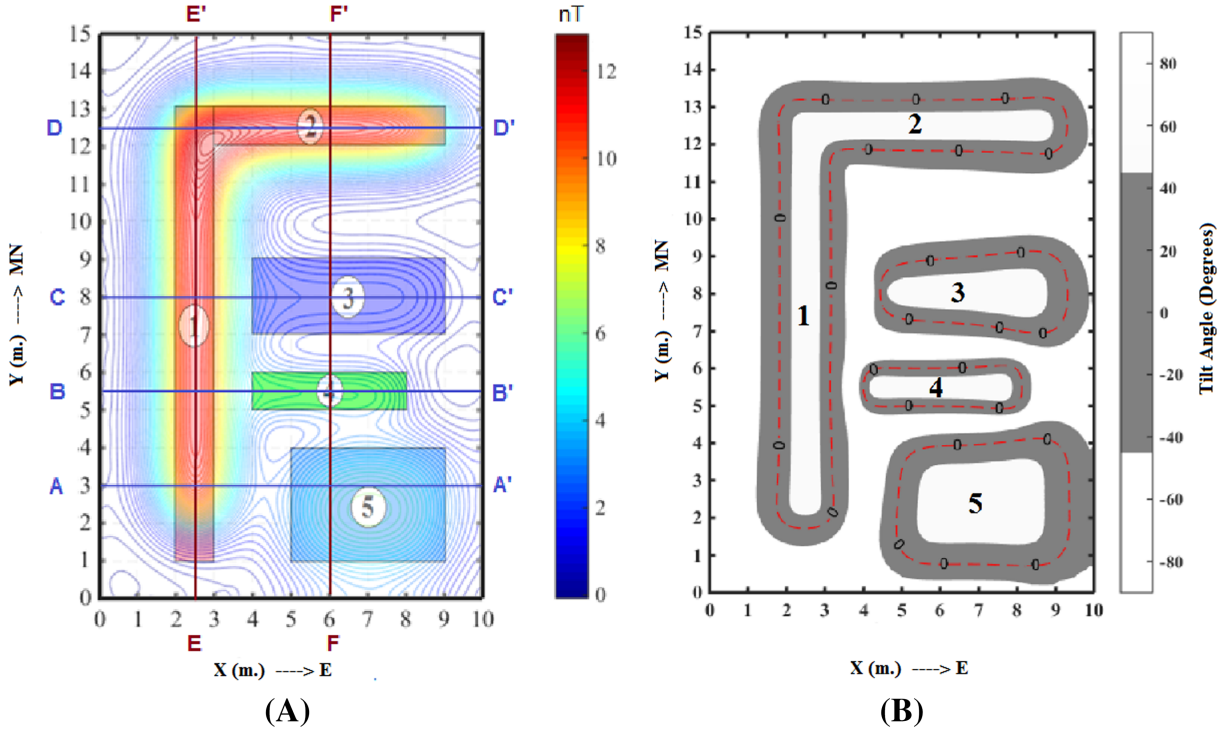

FIGURE 1 (A) Reduction to pole map (with model blocks and calculation profiles) and (B) tilt angle map of the synthetic model. Red dashed lines indicate the edges of the model blocks with the zero (0) contour [Color figure can be viewed at wileyonlinelibrary.com]

the wave numbers of different degrees and the wave numbers of different models is the change in the amplitude factor (structural index).

The iSPI method is susceptible to random noise. Although the method works well when the total area data are measured with high precision, the data to be used should still be processed carefully. Also, it is necessary to make sure that no noise is generated when calculating high-order vertical or horizontal derivatives. Carefully filtering the data used allows the local wave number to be estimated more accurately, and hence, the depth and structure index parameters are calculated more accurately. The automatic estimation of the depth and location of the effective sources that cause magnetic anomalies is done quickly and easily with the iSPI method.

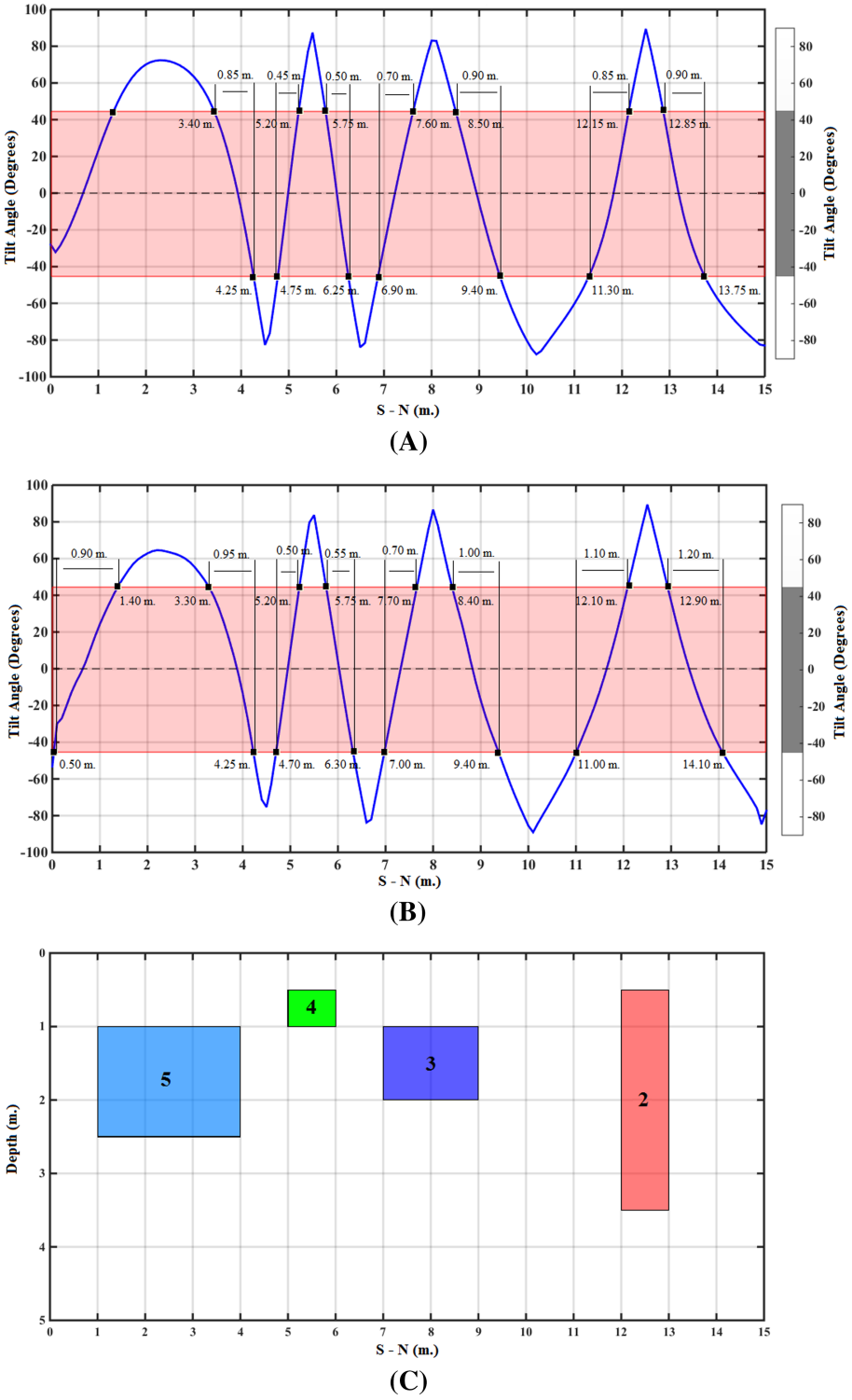

FIGURE 2 Tilt angle graphs of F–F' profile: (A) synthetic data without noise, (B) synthetic data with 0.3-nT standard deviation Gaussian noise, and (C) prismatic blocks encountered along the profile [Color figure can be viewed at wileyonlinelibrary.com]

3 | SYNTHETIC MODEL APPLICATIONS

Program codes were written in Matlab environment for TAD, SPI, and iSPI algorithms in order to determine the vertical boundaries of subsurface archaeological structures using field data. To test the usability of the prepared programs on the field data, the depth values obtained by making depth calculations on the synthetic archaeological model were compared with the actual model depth values. Using the theoretical total magnetic anomaly map reduced to the pole,[16] analysis of depth values of the blocks has been made on six of the profiles that were taken in the direction of West–East (A–A′, B–B′, C–C′, and D–D′ profiles) and in the direction of South–North (E–E′ and F–F′ profiles) (Figure 1A).

The zero (0) contours (red dashed lines) shown in Figure 1B give visual information about the horizontal edges of the blocks, and the distance between the contours (−45°, 45°) shown with a gray stripe gives visual information about the depth values of the model blocks. In the TAD method, half of the distance between the contours on the source boundaries (−45°, 45°) gives the depth values of the structures in question. As the distance between the contours (−45°, 45°) shown on the map increases, the top depth values of the effective sources increase, and as this distance decreases, the top depth values decrease at the same rate. In this context, the distance between the contours is relatively thin on the blocks 1, 2, and 4 with upper surface depths of 0.50 m, while the distances on the deeper blocks 3 and 5 are larger.

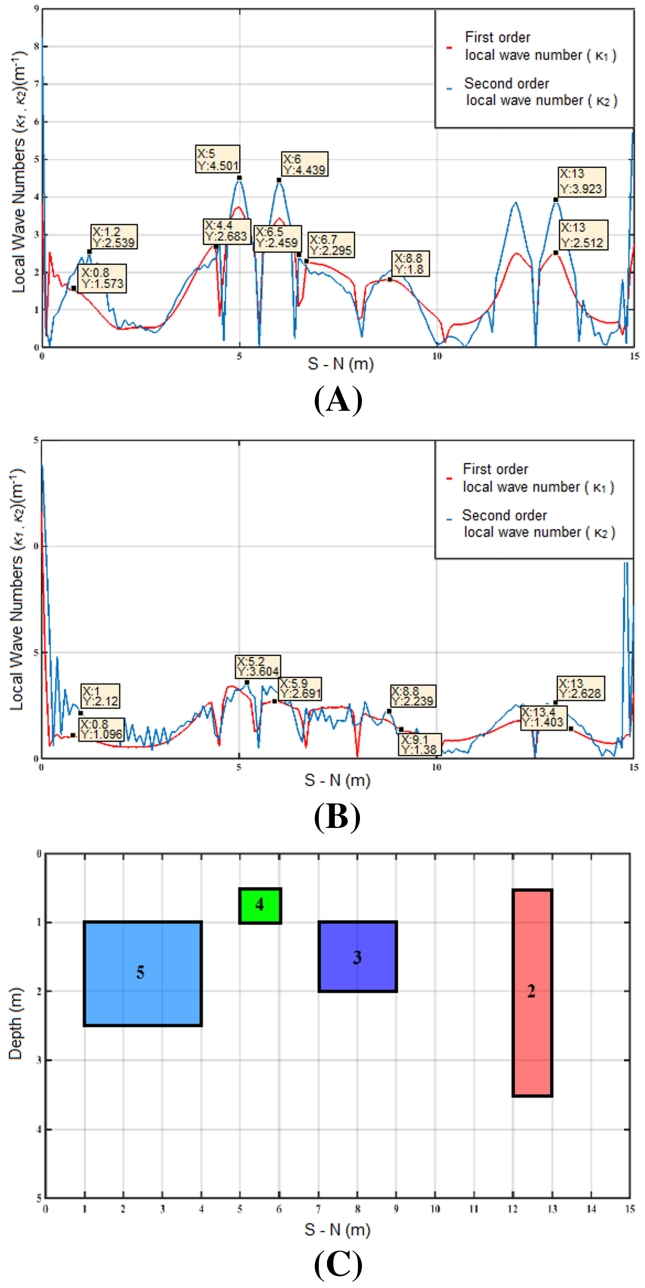

FIGURE 3 First- and second-order wave numbers of F–F profile. (A) Synthetic data without noise, (B) synthetic data with 0.3-nT standard deviation Gaussian noise, and (C) prismatic blocks encountered along the profile [Color figure can be viewed at wileyonlinelibrary.com]

Figure 2 shows the tilt angle graphs corresponding to model blocks of 2, 3, 4, and 5 in the F–F ′ profile for noise-free and the noisy data. According to the TAD method, for the synthetic data (without noise), the depth values of the model blocks were calculated 0.44, 0.40, 0.24, and 0.42 m, respectively. On the synthetic data graph, which is added Gaussian noise with a standard deviation of 0.3 nT, these values can be calculated as 0.57, 0.42, 0.26, and 0.46 m, respectively.

It has been concluded that this method can be used in determining the effective source boundaries in data analysis processes to be performed in archaeological sites using the tilt angle method. However, it cannot be used alone in depth calculations. It has been observed that if the subsurface effective source causing the anomaly is single, the relatively calculated depths can be reliable. In case of multiple sources, the calculated depths cannot be reliable. Among the reasons for this are the fact that the method is highly dependent on the quality of the data, the interactions of effective sources, and the resolution losses in the data due to the increasing depth values. Figure 3 shows the first- and second-order local wave number graphs corresponding to model blocks of 2, 3, 4, and 5 in the F–F' profile. According to the SPI method, for the synthetic data (without noise), depth values of the model blocks determined from first- and second-order local wave number values are 0.4, 0.56, 0.35, and 0.7 m. According to the iSPI method, these values are 0.71, 1.4, 0.55, and 1.03 m, respectively. On the synthetic data graph, which is added Gaussian noise with a standard deviation of 0.3 nT, these values can be calculated as 0.56, 0.72, 0.38, and 0.91 m (by SPI method) and 0.81, 1.09, 1.16, and 0.92 m (by iSPI method), respectively.

As a result of the SPI calculations, it can be said that the other block depths, except the third block, are compatible with the actual model depths despite the use of potential source data. In the case of the noise with the iSPI method, it can be

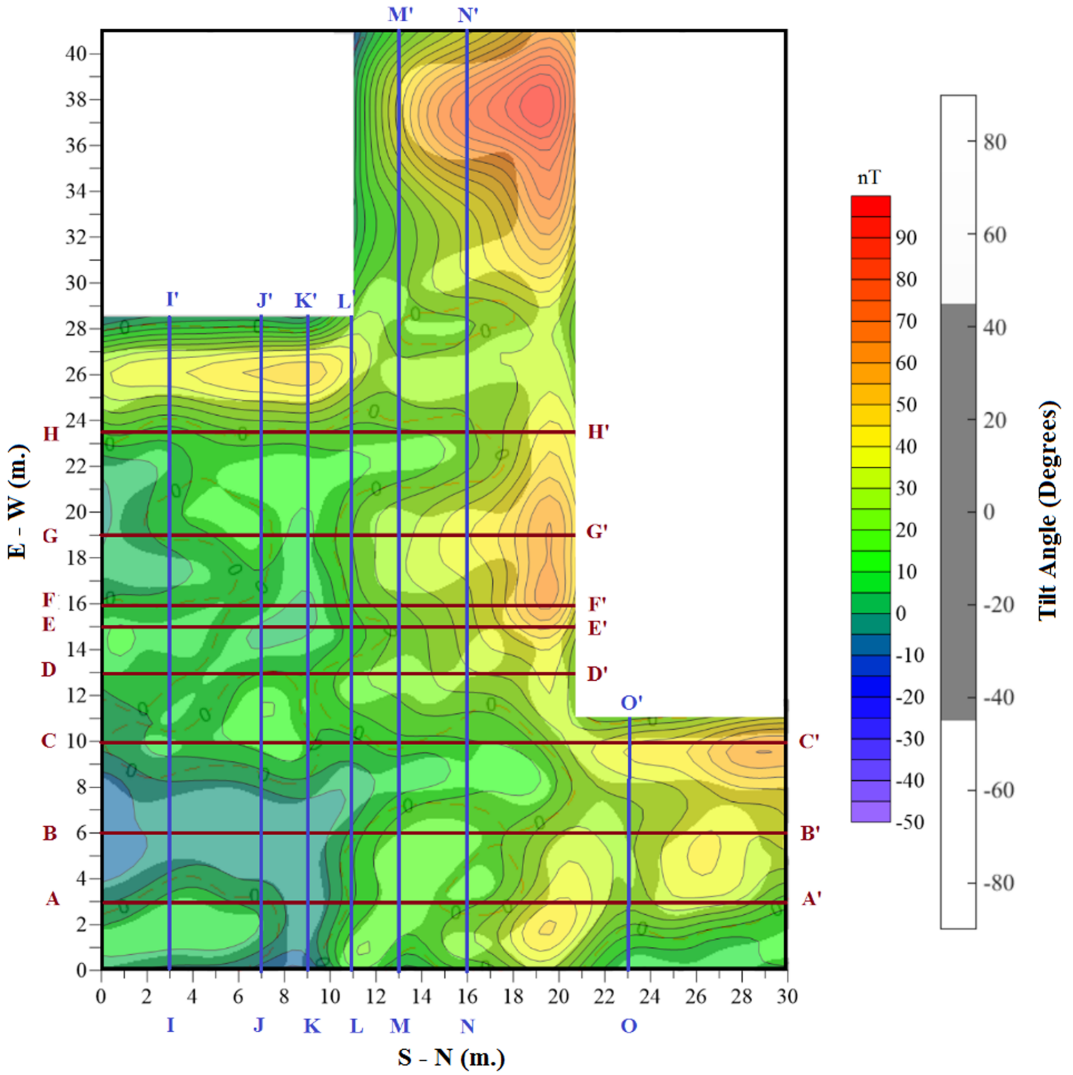

FIGURE 4 Amasya Oluz Mound total magnetic anomaly map (reduced to pole), tilt angle map, and depth calculation profiles [Color figure can be viewed at wileyonlinelibrary.com]

observed that the depth calculated for block 1 is not consistent with the actual value. In contrast, the depth of block 5 can be calculated substantially similar to the actual depth.

According to the calculated values, it can be seen that the depth values for the second block (noiseless and noisy data) and the third block (noisy data) are not compatible with the actual values of the blocks of the model. However, the calculated values of the other blocks are compatible with the actual model depths. It was observed that successful results were obtained by adding Gaussian noise to synthetic data to test the applicability of proposed algorithms to field data. Pole-reduced values were used as data during the application.

When the calculated values are examined, it is visible that the block depths obtained by the iSPI method are more consistent with the actual block depths, and the results obtained by the SPI method are partially consistent. When these criteria are taken into consideration, it is concluded that the results of iSPI and SPI methods, which are used, are reliable in the interpretation of the field data.

4 | FIELD APPLICATIONS

After determining the horizontal boundaries of the subsurface structure elements that cause magnetic data measured in the archaeological site of Amasya Oluz Mound,[16] the map given in Figure 4 was used to calculate the vertical depths of the subsurface structure elements that cause the same anomaly. The map consists of the overlapping total magnetic anomaly map of the region (reduced to the pole), the tilt angle map, and the profiles used in the calculation of the depths. The depth values of the subsurface structure elements on a total of 15 profiles in the direction of South–North and East–West were calculated for all three methods (TAD, SPI, and iSPI).

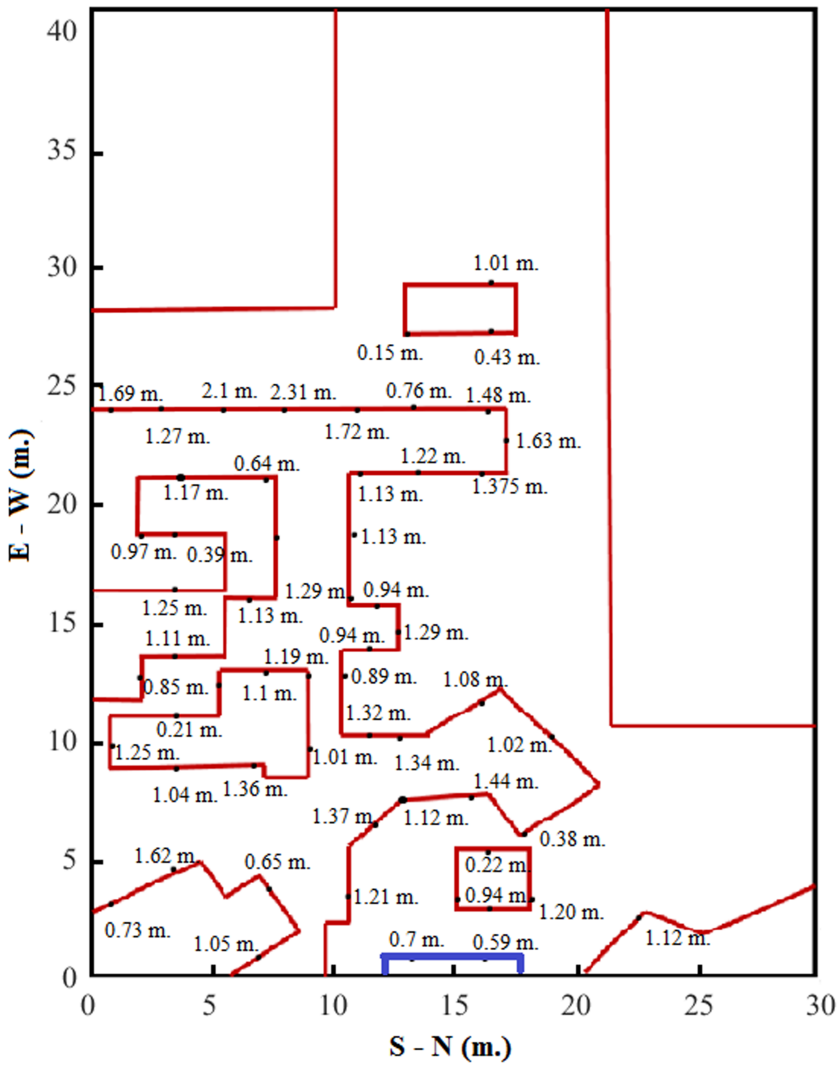

FIGURE 5 Map shows the simplified horizontal locations and vertical depths of the potential subsurface complex of the study area [Color figure can be viewed at wileyonlinelibrary.com]

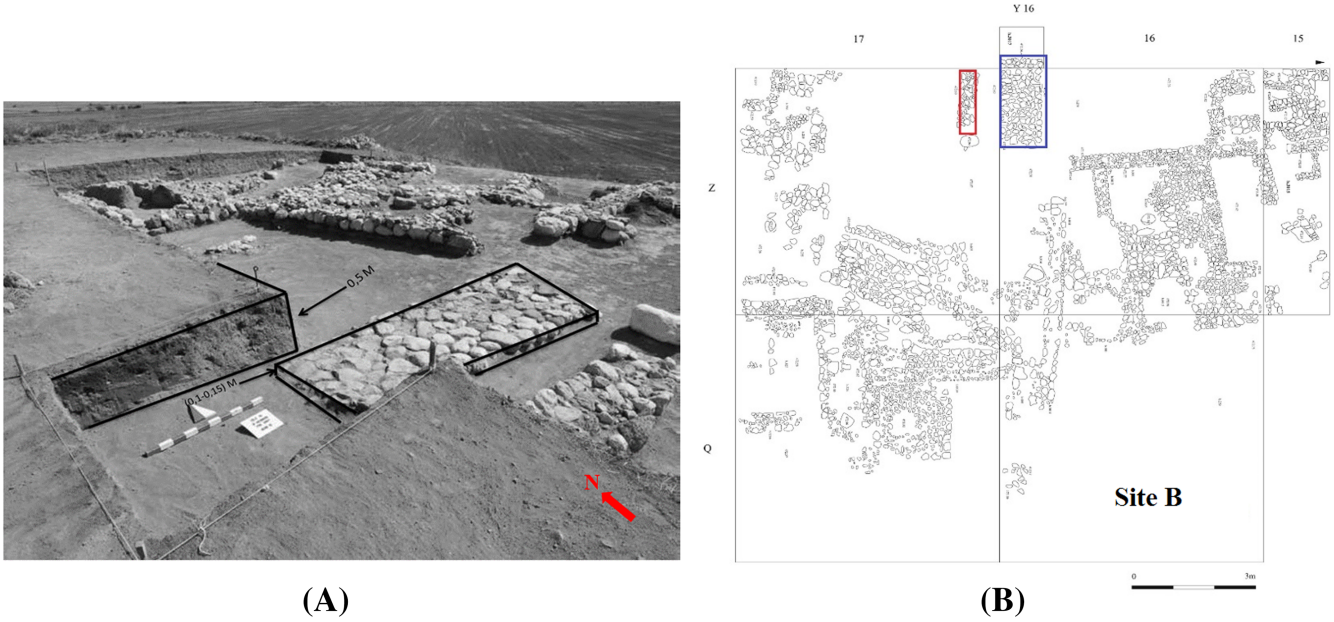

FIGURE 6 (A) Amasya Oluz-Höyük archaeological site, site B, first architectural layer remains,[17] (B) Amasya Oluz-Höyük archaeological site B grids Z 15, Z 16, Z 17, Q 15, Q16, Q17, and Y16[17] [Color figure can be viewed at wileyonlinelibrary.com]

The locations of potential subsurface archaeological structure distributions that cause anomalies have been revealed by applying the tilt angle and automatic gain control methods to the field data. In the Tilt Angle map, the places where the zero (0) contour passes are assumed to be the horizontal locations of potential buried archaeological structure elements. Architectural building foundations giving corner shape in the region and road routes between these foundations were visualized. These routes, which do not have linear features, are probably covered with architectural stone debris. When the potential subsurface source boundaries that cause the anomaly on the map shown in Figure 5 are examined, it is seen that the settlement is concentrated in the southeast direction of the map. Locations with zero contours on the tilt angle map of the region were accepted as potential building boundaries, and the depth values at these points were calculated for all three methods. Graphs of the methods were created on the specified profiles, and the depth values of the potential structure in the region were calculated with the values obtained from the graph values as shown in the synthetic model calculations. In line with these values, a simplified depth map of the area was created, and the numerical values were shown on the map in this area, which is located between sites B and C opened in the previous years and has not yet started excavation (Figure 5).

As a result of the expansion works towards the west of Site B, which was opened in 2015 in the study area (Figure 6A), it was determined that the stone-paved road remains with a depth of 0.5 m and continues for 0.5 m, which is thought to extend to the building complex from the west direction, and corresponds to the area shown in blue in Figure 6B. Depth values of potential archaeological structure elements in this region calculated from SPI and iSPI methods are 0.7 and 0.59 m. It can be said that the depth values calculated using these methods are compatible with the depth of the foundation structure determined as a result of the expansion studies. Potential subsurface building boundaries shown in red in Figure 5 are considered to be the continuation of the road route shown in red on grid squares in Figure 6B.

5 | CONCLUSIONS

Numerical analyses of potential structures were performed using derivative-based methods to calculate the horizontal location and depth values of potential subsurface structures that cause anomalies on magnetic anomaly maps. Derivative-based methods are used for depth calculations in the process of numerical analysis of magnetic data. In this context, the programs prepared by writing codes in Matlab environment belong to the derivative-based methods such as TAD, SPI, and iSPI planned to be used in field data, were applied to the theoretical data. With these three methods (using

horizontal and vertical derivatives of the magnetic field), the depth values of the model blocks were calculated over six profiles, and the results were examined. It has been observed that the TAD method calculates the depth of blocks close to the surface more accurately compared to the depth values of the structures located deeper, whereas the SPI and iSPI methods give more successful results at every depth. It can be said that the iSPI method is more sensitive to noise because it includes second-order derivatives. In general, it was seen that all three methods were calculated close to the depth values of the model blocks selected in the synthetic study. As a result, it was decided that these three methods can be applied to the field data.

To determine the potential subsurface source depths that cause an anomaly in the study area, which has not been opened yet, calculations were made along 15 profiles on the field data by using the methods of TAD, SPI, and iSPI. By comparing the results of all three methods, it was concluded that the depth values of the structure distributions varied between 0.45 and 2 m. These structures could be floor and wall bases moving towards the west of site B, opened in the region.

As a result, programs were written to be applied in archaeological studies and applied to archaeogeophysical data by using the algorithms of the methods proposed in this study of the historical heritage previously determined in the archaeological area of the Oluz Mound region of Amasya. Using these methods, the horizontal position parameters and depth values of the potential historical settlement were analyzed numerically. A preliminary study was carried out to shed light on the planning of the archaeological excavations, which are planned to be carried out to uncover the historical heritage in the relevant area by obtaining maps of potential subsurface archaeological structures by using the calculated geometric parameters.

ACKNOWLEDGEMENT

The authors would like to express their gratitude to Şevket Dönmez and the excavation crew for enabling us to apply geophysical methods in the excavation site.

ORCID

Hazel Deniz Toktay https://orcid.org/0000-0002-3806-489X
Davut Aydoğan https://orcid.org/0000-0001-8792-2099
Fethi Ahmet Yüksel https://orcid.org/0000-0003-2207-1902

REFERENCES

1. Thompson DT. EULDPH: A new technique for making computer-assisted depth estimates from magnetic data. *Geophysics*. 1982;47(1):31-37.
2. Gupta OP. A least-squares approach to depth determination from gravity data. *Geophysics*. 1983;48(3):357-360.
3. Sailhac P, Gibert D. Identification of sources of potential fields with the continuous wavelet transform: Two-dimensional wavelets and multipolar approximations. *J Geophys Res Solid Earth*. 2003;108(B3):2262-2270.
4. Fedi M. DEXP: A fast method to determine the depth and the structural index of potential fields sources. *Geophysics*. 2007;72(1):1-11.
5. Thurston J, Smith R. Source location using total-field homogeneity: Introducing the SLUTH method for depth estimation. *Lead Edge*. 2007;26(10):1272-1277.
6. Fedi M, Florio G, Smith R. Determination of the maximum-depth to potential field sources by a maximum structural index method. *J Appl Geophys*. 2013;88:154-160.
7. Miller H, Singh V. Potential field tilt—a new concept for location of potential field sources. *J Appl Geophys*. 1994;32(2):213-217.
8. Verduzco B, Fairhead JD, Green CM, MacKenzie C. New insights into magnetic derivatives for structural mapping. *Lead Edge*. 2004;23(2):116-119.
9. Salem A, Williams S, Fairhead JD, Ravat D, Smith R. Tilt-depth method: A simple depth estimation method using first-order magnetic derivatives. *Lead Edge*. 2007;26(12):1502-1505.
10. Nabighian MN. The analytic signal of two-dimensional magnetic bodies with polygonal cross-section; its properties and use for automated anomaly interpretation. *Geophysics*. 1972;37(3):507-517.
11. Thurston JB, Smith RS. Automatic conversion of magnetic data to depth, dip, and susceptibility contrast using the SPI (TM) method. *Geophysics*. 1997;62(3):807-813.
12. Bracewell NR. *The Fourier Transform and its Applications*. New York: McGraw-Hill Book Co.; 1965.
13. Smith RS, Thurston JB, Dai TF, MacLeod IN. iSPITM— the improved source parameter imaging method. *Geophys Prosp*. 46(2):141-151.

14. Murthy KSR, Mishra DC. Fourier transform of the general expression for the magnetic anomaly due to a long horizontal cylinder. *Geophysics*. 1980;45(6):1091-1093.
15. Redford MS. Magnetic anomalies over thin sheets. *Geophysics*. 1964;29(4):532-536.
16. Toktay HD, Aydofan D, Yüksel FA. Quantitative analysis of total magnetic anomaly maps on archaeological aites - Part1, submitted. *Math Meth Appl Sci*. 2021.
17. Dönmez Ş, Beyazıt AY. Oluz Höyük Kazısı Dokuzuncu Dönem (2015) Çalışmaları: Değerlendirmeler Ve Sonuçlar (in Turkish) In: 38. Kazı Sonuçları Toplantısı: Edirne, 2016, 537–552

How to cite this article: Deniz Toktay H, Aydoğan D, Yüksel FA. Quantitative analysis Of total magnetic anomaly maps on archaeological sites—Part 2. *Math Meth Appl Sci*. 2021;1-12. https://doi.org/10.1002/mma.7651